Measurement of the Exclusive $D^0\overline{D}^0$ Production Cross Section from e^+e^- Collisions at 4.03GeV

by

Vicentica Valdes

B.S., Nuclear Engineering
University of California, Berkeley, 1993

Submitted to the Department of Physics in Partial Fulfillment of the Requirements for the Degree of Master of Science in Physics

at the
Massachusetts Institute of Technology
February 1997

Signature of Author: _____
Department of Physics
January 17, 1997

Certified by: _____
Richard K. Yamamoto
Professor of Physics
Thesis Supervisor

Accepted by: _____
George Koster
Professor of Physics
Chairman, Graduate Committee

Measurement of the Exclusive $D^o\overline{D}^o$ Production Cross Section from e^+e^- Collisions at 4.03GeV

by

Vicentica Valdes

Submitted to the Department of Physics on January 17, 1997

in partial fulfillment of the requirements

for the degree of Master of Science

Several measurements of the inclusive $D^o\overline{D}^o$ production cross section have been made in the past 15 years, mainly from data collected by the MARK II detector at SPEAR. Most of these measurements were done at the $\Psi^{''}(3770)$ resonance, which is just above the pair production threshold of $D^o\overline{D}^o$. A measurement of the exclusive $D^o\overline{D}^o$ production cross section in the energy range of $(4.02-4.15)GeV$ was made in 1982 with data from Mark II, resulting in $\sigma_{D\overline{D}} = (0.3 \pm 0.3)nb$. Here, we have measured this exclusive production cross section at a center-of-mass energy of $4.03GeV$, with data obtained from $27pb^{-1}$ of integrated luminosity. These data were collected with the Beijing Spectrometer at the Beijing Electron Positron Collider. We double-tag the $D^o \rightarrow K^-\pi^+$ decay mode, scale by the known decay branching fraction and obtain $\sigma_{D\overline{D}} = (0.91 \pm 0.31)nb$.

Thesis Supervisor: Richard K. Yamamoto
Title: Professor of Physics

Table of Contents

List of Figures

List of Tables

1. Motivation

1.1. Introduction

The quark composition of the mesons in this analysis is shown in Table 1.1-1. The D^o meson has a quark composition of $(c\bar{u})$, and $(u\bar{c})$ for $\overline{D}^o$. Table 1.1-2 lists quark information. We chose the $D^o \rightarrow K^-\pi^+$ decay mode because it has charged particles that the detector is tailored to find, and because it has a rather large branching fraction [1] compared to other two-body decay modes (see Table 1.1-3).

TABLE 1.1-1 Meson Information

Meson	Quark Composition	Mass (*MeV*)	c*Lifetime	$I(J^P)$
D^o	$c\bar{u}$	1864.6 ± 0.5	$124.4\mu m$	$\frac{1}{2}(0^-)$
D^{*o}	$c\bar{u}$	2006.7 ± 0.5	$\Gamma < 2.1 MeV$	$\frac{1}{2}(1^-)$
D^+	$c\bar{d}$	1869.4 ± 0.4	$317\mu m$	$\frac{1}{2}(0^-)$
D^{*+}	$c\bar{d}$	2010.0 ± 0.5	$\Gamma < 0.131 MeV$	$\frac{1}{2}(1^-)$
K^+	$u\bar{s}$	493.677 ± 0.016	$3.709m$	$\frac{1}{2}(0^-)$
π^+	$u\bar{d}$	139.56995 ± 0.00035	$7.804m$	$1^-(0^-)$
π^o	$\frac{1}{\sqrt{2}}(u\bar{u} - d\bar{d})$	134.9764 ± 0.0006	$25.1\mu m$	$1^-(0^{-+})$

TABLE 1. 1-2 Quark Information

Quark	Mass	Charge / e	$I(J^P)$
u	2 to 8 *MeV*	2/3	$1/2(1/2^+)$
d	5 to 15 *MeV*	−1/3	$1/2(1/2^+)$
s	100 to 300 *MeV*	−1/3	$0(1/2^+)$
c	1.0 to 1.6 *GeV*	2/3	$0(1/2^+)$
b	4.1 to 4.5 *GeV*	−1/3	$0(1/2^+)$
t	>62 *MeV*	2/3	$0(1/2^+)$

TABLE 1.1-3 D^0 Decay Mode Information

D^0 Decay Products	Branching Fraction
$K^-\pi^+$	$(4.01 \pm 0.14)\%$
K^-K^+	$(4.54 \pm 0.29) \times 10^{-3}$
$\pi^-\pi^+$	$(1.59 \pm 0.12) \times 10^{-3}$
$K^+\pi^-$	$(3.1 \pm 1.4) \times 10^{-4}$
$K^-\pi^+\pi^0$	$(13.8 \pm 1.0)\%$
$K^-e^+\nu$	$(3.8 \pm 0.22)\%$
$K^-\mu^+\nu$	$(3.2 \pm 0.4)\%$

1.2. Previous Measurements

Several measurements have been made to determine the exclusive $D^o\overline{D}^o$ cross section, denoted herein by $\sigma_{D\overline{D}}$. Note that the current value of the branching fraction for the $K^-\pi^+$ decay mode of the D^o meson is $B(D^o \rightarrow K^-\pi^+) = 0.0401 \pm 0.0014$. For the most part, measurements were made at the $D^o\overline{D}^o$ threshold ($\Psi''(3770)$), meaning that the observed neutral D mesons were assumed to occur only as primary mesons via $e^+e^- \rightarrow D^o\overline{D}^o$. We can, at the least, use these results as an upper limit on $\sigma_{D\overline{D}}$.

In 1981, the Mark II detector measured the exclusive $D^o\overline{D}^o$ pair production cross section at the $\Psi''(3770)$ resonance, corresponding to a center-of-mass energy of $3.771 GeV$. The analysis yielded $\sigma_{D\overline{D}} B(D^o \rightarrow K^-\pi^+) = 0.24 \pm 0.02$. Using the current branching fraction above, this gives an exclusive cross section of $\sigma_{D\overline{D}} = (5.99 \pm 0.25) nb$. Although this analysis was done at the $D^o\overline{D}^o$ threshold, it provides a check for our analysis. [2]

In 1982, data from the Mark II detector at SPEAR was analyzed to find an exclusive $D^o\overline{D}^o$ production cross section at a center-of-mass energy between $(4.02 - 4.15) GeV$ of $\sigma_{D\overline{D}} = (0.3 \pm 0.3) nb$, via the $K^-\pi^+$ decay mode. This was determined with single-tags of the D^o mesons and an efficiency determined using an isotropic angular distribution for the generated D^o mesons. An anisotropic efficiency (using the angular distribution

$dN/d\Omega \sim 1 \pm \cos^2\theta$, where θ is the angle between the momentum of the D^o meson and the e^+ beam) yielded $\sigma_{D\bar{D}} = (0.2^{+0.3}_{-0.2})nb$. The analysis was done using a branching fraction for the $K^-\pi^+$ decay mode of $B(D^o \to K^-\pi^+) = 0.03 \pm 0.006$. [3]

In 1986, the Mark III collaboration performed several measurements at the $\Psi''(3770)$ resonance. The D^o mesons were double-tagged, giving $\sigma_{D\bar{D}} = (4.48^{+0.33}_{-0.29} \pm 0.37)nb$, the first error being statistical and the second, systematic. [4]

Note that with BES, we do have the largest volume of available data, even after throwing out $4.3pb^{-1}$ of integrated luminosity with useless dE/dx information. In addition, recall that for measurements done at the resonance, it was assumed that D^o mesons were always primary mesons.

TABLE 1.2-1 Summary of Previous Measurements

Detector	Year	$E_{C.M.}$ (*GeV*)	Integrated Luminosity (pb^{-1})	Reported Measurement (nb)	$\sigma_{D\bar{D}}$ (nb) with 1994 Branching Fraction
MARK II	1981	3.771	2.85	$\sigma_{D\bar{D}} B(D^o \to K^-\pi^+) = 0.24 \pm 0.02$	5.99 ± 0.25
MARK II	1982	4.02 – 4.15	0.906	$\sigma_{D\bar{D}} = 0.3 \pm 0.3$	0.2 ± 0.2
MARK III	1986	3.770	9.558	$\sigma_{D\bar{D}} = 4.48^{+0.33}_{-0.29} \pm 0.37$	6.26 ± 1.26

1.3. Objective

The objective of this analysis is to measure the exclusive $D^o\bar{D}^o$ production cross section at a center-of-mass energy of $4.03GeV$. This would add to the world's measurements of $D^o\bar{D}^o$ production cross sections as a function of energy.

2. Instrumentation

2.1. Description of the Beijing Electron Positron Collider

The Beijing Electron Positron Collider (BEPC) is located at the Institute of High Energy Physics (IHEP) in Beijing, China.

The primary objective of the BEPC is to study the physics of charm quarks and tau leptons via mesons produced by e^+e^- annihilations at center-of-mass energies from 3.0 to 5.6 *GeV*. Since January of 1990, when the collider was first operational, the BEPC had collected nine million J/Ψ events. [5]

The BEPC [6] is shown schematically in Fig. 2.1-1. After the electrons pass through the pre-injector and the positron production target, both electrons and positrons are accelerated in the main linac to energies between 1.1 and 1.4 *GeV*. The beam intensity of the electrons is about 66 times greater than that of the positrons. The electrons and positrons are then separated by a magnet and pass through their respective transport tunnels to the injection points of the storage ring, where they are further accelerated to steady beam energies between 1.5 and 2.2 *GeV*.

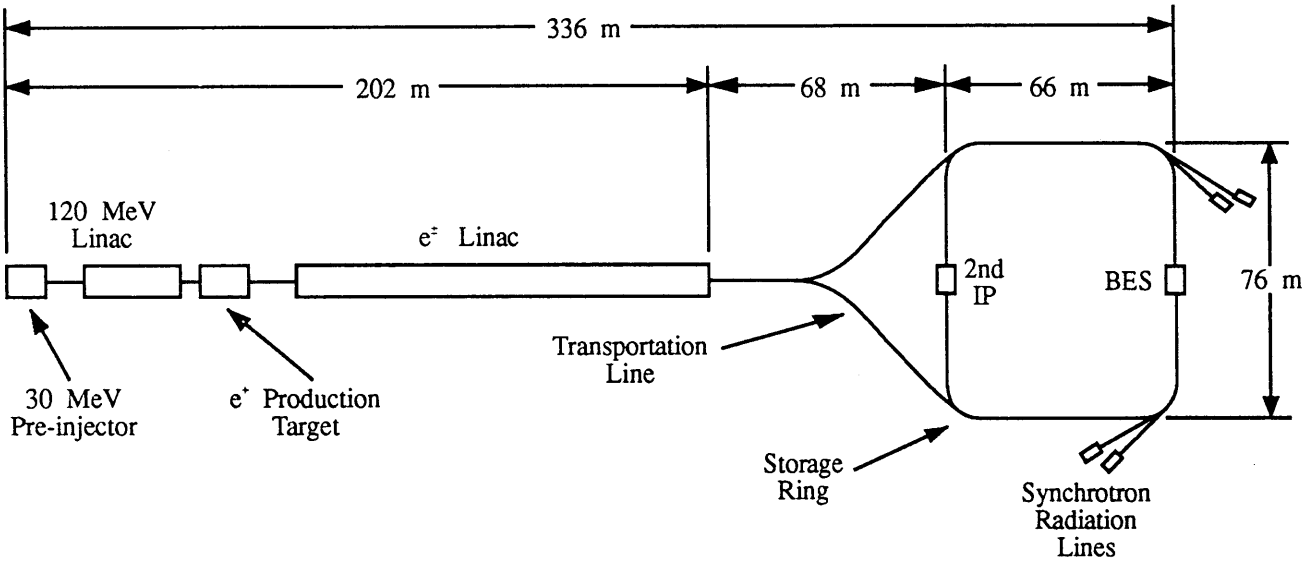

Figure 2.1-1. BEPC schematic

The storage ring is made up of 4 arcs, with a circumference of 240.4 meters, with two interaction regions at diametrically opposite points. Bunches of particles from each beam collide with a frequency of 1.25*MHz*. Although typical luminosities for this experiment at a center-of-mass energy of $4.03GeV$ were typically between 1 and 2 x $10^{30} cm^{-2} s^{-2}$, it

peaked at 8 x $10^{30} cm^{-2} s^{-2}$. The detector was positioned at one of the two interaction regions of the storage ring (the other site remaining unoccupied for this experiment).

2.2. Description of the Beijing Spectrometer

The Beijing Spectrometer (BES) is shown schematically in Figs. 2.2-1 and 2.2-2. The design was such as to optimize detection for charged particles although it has capabilities to detect certain neutral particles. From the center out, radially, BES consists of the beam pipe, the central drift chamber (CDC), the main drift chamber (MDC), the time of flight counter (TOF), the barrel shower counter (BSC), the magnet coil, the iron yoke and the muon counter. It has luminosity monitors right next to the beam pipe which also detect small angle Bhabha scattering (elastic e^+e^- scattering), an endcap shower counter, an endcap TOF counter and quadrupole final-focusing magnets at the electron and positron entrance points.

The data used in this analysis were obtained from the MDC and the TOF system, but not the TOF endcaps that had not been properly calibrated for this experiment.

2.2.1 The Beam Pipe

The beam pipe is made from aluminum with an outer diameter of $150mm$ and a wall thickness of $2mm$. The thinness and low atomic number of the material, corresponding to 2.25 x 10^{-2} radiation lengths, is desired in order to decrease multiple scattering of charged particles.

2.2.2. The Central Drift Chamber

The CDC is a small version of the MDC. It is right outside of the beam pipe and has four layers, each consisting of 48 sense wires for trajectory tracking purposes. Its main purposes are to assist the MDC in accepting track trajectories, define a trigger for an event and to reduce the cosmic ray background. The gas mixture used in the CDC is $Ar / CO_2 / CH_4 = 89\% / 10\% / 1\%$. The CDC has a single-wire position resolution of $220\mu m$ in the $r - \varphi$ plane, planes perpendicular to the beams, and an $8.8mm$ resolution along the z, the direction of the beam.

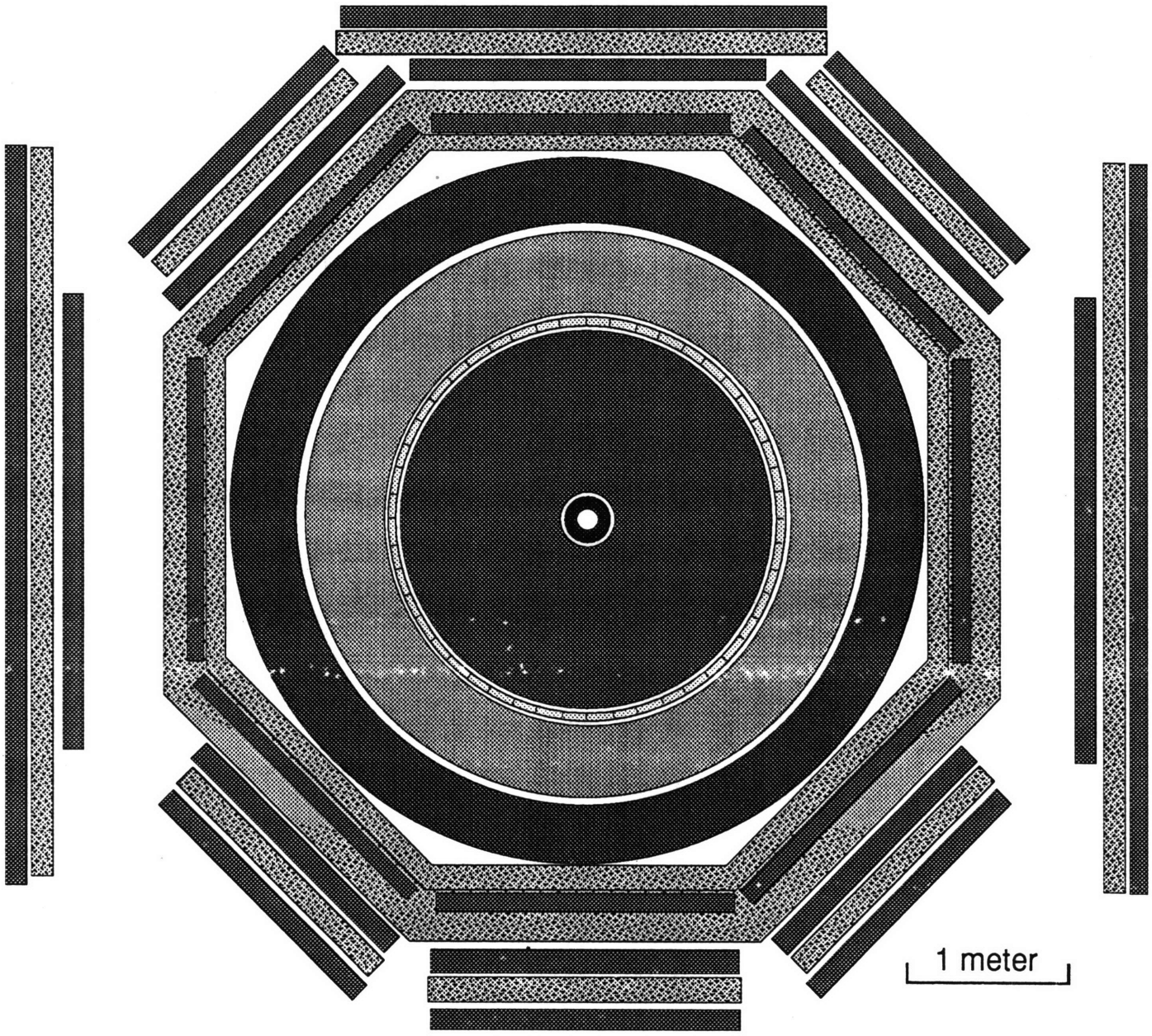

Figure 2.2-1. An axial view of BES

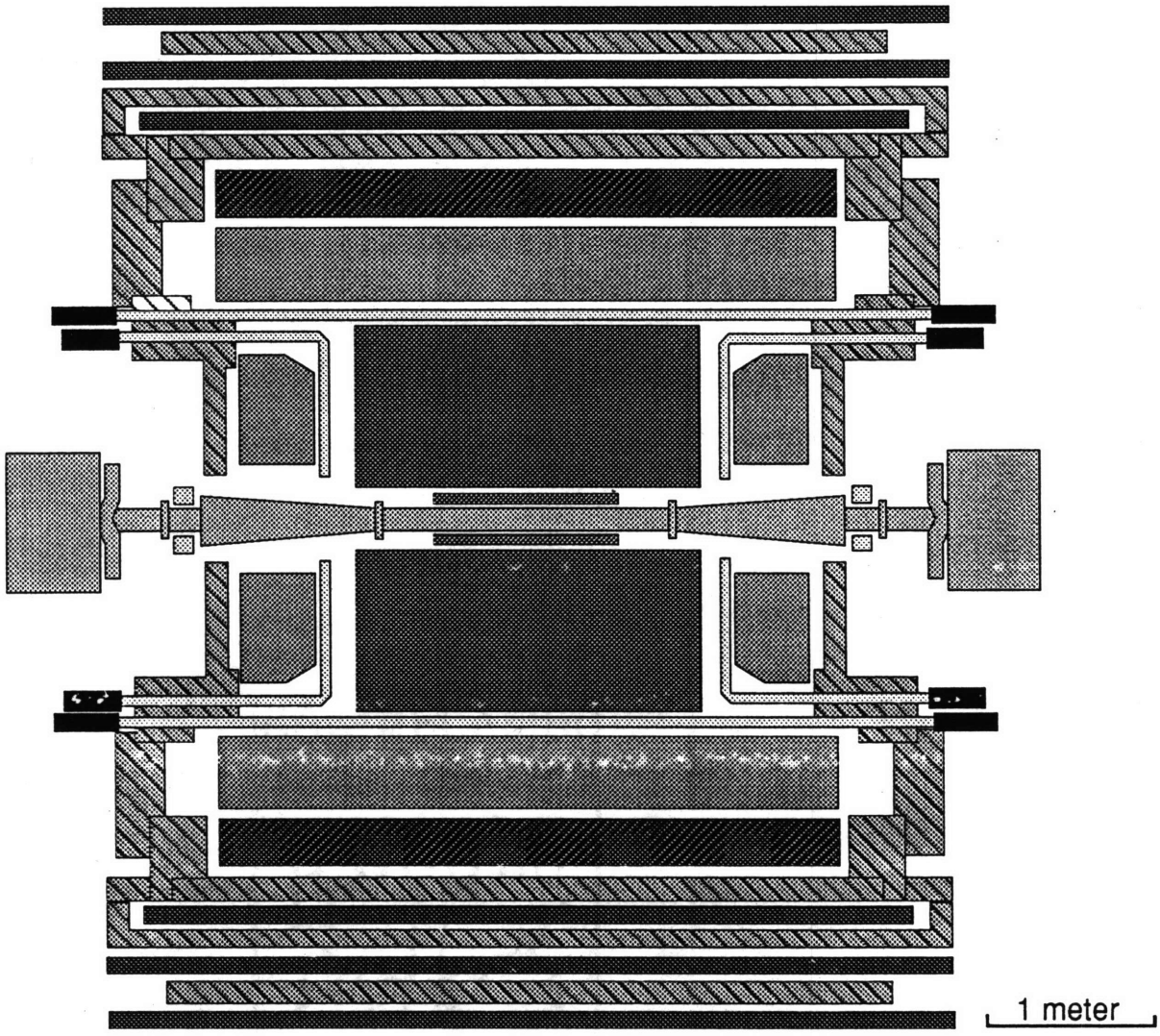

Figure 2.2-2. A side view of BES

2.2.3. The Main Drift Chamber

This is the primary component of BES and where the majority of the data for this analysis comes from. The MDC measures the momenta and the trajectory of charged particles as well as their ionization loss, in order to determine dE/dx [7] for particle identification. Located immediately outside the CDC, the MDC has ten tracking layers.

Each tracking layer has a varying number of cells, increasing with the radial distance from the center. The tracking layers alternate with one layer having cells with sense wires parallel to the axis of the chamber and the next two layers having cells with wires at slight positive and negative angles with respect to this axis (stereo layers). The stereo layers provide information to determine the track coordinates along the z axis. This is done by measuring distances of track hits from the stereo wires of opposite angles and computing z from the known geometry.

Each of the wedge-shaped cells contain four sense wires. The signals from these sense wires can be used to determine dE/dx (which depends on the amount of charge collected by the sense wires) and the position of the track trajectory (via the drift time). The electric field must be maintained as constant as possible throughout the volume of each cell in order to maximize the spatial resolution, sustain uniformity of the dE/dx data collecting process, and facilitate reconstruction of tracks.

The MDC uses a gas mixture of $Ar / CO_2 / CH_4 = 89\% / 10\% / 1\%$, the same as in the CDC. The gas is ionized by charged particles traversing the MDC. The ionization electrons then drift through the cell's uniform electric field toward the sense wires. The high electric field near the sense wire causes high acceleration of primary electrons, which in turn cause further ionizations, resulting in an avalanche. This provides a signal whose pulse height depends on the amount of charge collected, and whose arrival determines a drift time. These drift times, in conjunction with the known drift velocity, imply the location of the primary ionization, and that in turn can be used to determine the trajectory of the charged

particle. The trajectory's radius of curvature (R) from the magnetic field (B) then gives us the momentum, $p = qBR$.

The MDC has a maximum solid angle coverage of 95% of 4π in the second layer, decreasing to 70% of 4π in the tenth (outermost) tracking layer. The $r-\varphi$ plane single-wire position resolution remains between 200 and 250 μm throughout the MDC and the momentum resolution is $\frac{\Delta p}{p} = 0.017\sqrt{1+p^2}$ (p in GeV/c).

2.2.4. The Time of Flight System

The barrel TOF consists of 48 scintillation counters, mounted on the outside of the MDC and provide a solid angle coverage of 76% of 4π. Each scintillator is $2840mm$ in length along the beam axis, $156mm$ wide and $50mm$ thick. Each one is connected to light guides at both ends, and the light guides are attached to photomultiplier tubes. Although the endcap TOF covers 20% of 4π, data from it was not used in this analysis. The TOF performance is periodically monitored by a laser apparatus.

The TOF is the time it takes a particle to travel from its production point in the e^+e^- 'collision' to its point of detection at the scintillator counter. The collision time, or beam crossing time, is determined by electrodes adjacent to the beam pipe. The electrodes detect the passing bunches that are about $5cm$ in length. The overlap in the bunches of about $170ps$ contribute to the uncertainty in the TOF measurement. For this experiment, the resolution of the TOF was between 400 and $500ps$. This included the effects of aging scintillation counters.

2.2.5. The Shower Counter

The barrel shower counter (BSC) is sandwiched by the TOF and the solenoid. It is constructed of 24 absorbing layers consisting of thin instrumented aluminum layers encasing a thin sheet of lead. The aluminum layers have cells with sense wires in a gas mixture ($Ar / CO_2 = 34\% / 66\%$). The purpose of the shower counter is primarily to detect and determine the energy of particles that react electromagnetically, namely of photons and electrons. Data from the BSC was not usable in this study.

2.2.6. The Magnet

The magnet consists of the 0.4 Tesla solenoidal coil mounted within an iron yoke that serves as the main support for BES, as well as the flux return path and muon filter for the muon counter.

2.2.7. The Muon Counter

Located at the outermost part of the detector is the muon counter. It is made up of three layers of aluminum chambers (with 8 proportional counters in each) and three layers of absorbers. The absorbers are made of octagonal yoke of varying thicknesses. Because the muons have a very low probability of nuclear interactions, they leave a clean track through the muon counter. This can be compared to the track left by pions, which have a relatively higher probability of interacting with the system of alternating layers of iron and scintillators in this component. The muon counter is used to veto events with positively identified muons.

3. Data Acquisition

3.1. Triggering

Triggering allows data to be recorded while limiting the amount of frivolous background. The desired set of data would consist of charmed events and calibration events. Calibration of the luminosity monitors and the detector itself was done primarily with wide-angle Bhabhas and muon pairs.

Charm events and Bhabhas (for calibration) are characterized as those having high momentum tracks, determined from at least two tracks in the MDC and their associated TOF hits, and large ionization losses, determined via detection of at least $1GeV$ of total energy deposition in the BSC. Muon events for calibration are characterized as those having at least one hit in the innermost layer of the muon counter. A trigger is defined by having met any one of the above criteria. With a $1.25MHz$ bunch collision rate, the trigger rate was typically 5-10 Hz.

3.2. Experimental Runs

The data used in this analysis was provided by the University of Dallas, Texas on an NDST formatted tape (utd.0145), used with the v87 BES code. The tape contained runs from 1992, 1993 and 1994. [6]

The total integrated luminosity collected in 1992 was $3.3pb^{-1}$. However, two-thirds of the data was collected with a time-to-amplitude converter for the drift chamber with its threshold set too high. This reduced the triggering efficiency as well as the efficiency for track reconstruction in those events that made it past the trigger. The problem was corrected for the remaining third of the data; thus, two sets of Monte Carlo simulations for the data analysis were required.

The 1993 data set contained good dE/dx information for $4.7pb^{-1}$ out of a total of $7.3pb^{-1}$ of integrated luminosity. The remaining dE/dx information in the data was corrupted due to a problem in the pulse heights, obtained from the drift chamber.

In 1994, the most productive year, BES collected a total of $14.7pb^{-1}$ of integrated luminosity. Although this data had a systematic error in the beam center-of-mass energy ($4.03GeV$) of $\sim \pm 2MeV$, it was negligible in the final analysis.

4. Monte Carlo Simulation

4.1. General Approach

The BES software provided a Monte Carlo package for the physics and the detector response to the physics. It was used to simulate the $D^{o}\overline{D}^{o}$ signal and the background, as well as for the calculation of efficiencies and determination of kinematic cuts for the reduction of background.

The charm physics was simulated using accepted modes for angular distributions of decay products and accepted charmed meson decay branching fractions. The detector simulation was done with actual calibration measurements (primarily with such well established processes as J/Ψ and Ψ'' decay channels), taking into account particle interactions with the various materials used in the construction of BES.

We determined an efficiency as a function of the angular coordinates (the azimuthal angle, φ, and the polar angle, θ) of the neutral D meson candidate that included the loss of data due to kinematic cuts in the momentum, the invariant mass, and the back-to-back angle of the D^o meson pairs. This accounted for the response of the detector to double-tagging the D^o meson pairs decaying to our selected mode. The efficiencies were then just the ratio of the number of D^o meson pairs that were successfully reconstructed to the number that were generated.

4.2. *D* Meson Physics Simulation

The D meson simulation began with decays of $4.03GeV$ Ψ'' to D^o mesons that subsequently decayed to the longer lived states (pions, kaons, leptons, and photons). These were then "allowed to travel" through the simulated detector. The $D^o\overline{D}^o$ samples were allowed to decay using well-established branching fractions. Additionally, because our sample consisted of "interesting events" at $4.03GeV$, we looked at Monte Carlo samples consisting of all primary modes subsequently producing D^o mesons at $4.03GeV$.

4.3. Angular Efficiencies

The angular efficiencies, $\varepsilon(Cos\,\theta_D, \phi_D)$, were determined by looking at the dependence on the angular coordinates of the D^o meson The Monte Carlo allowed D^o mesons to decay into pions and kaons with random directions that propagated through the detector. We reconstructed the angular coordinates for those $D^o\overline{D}^o$ pairs whose $K\pi$ decay products were successfully detected. A large sample of these events (50,000 events per data set) were generated to provide a solid angle mapping, subject to kinematic cuts, of the efficiency with a relatively small statistical error. Then $\varepsilon(Cos\,\theta_D, \phi_D)$ was the ratio of successfully detected events to the number of generated events per $\Delta\Omega = \Delta Cos(\theta)\Delta\varphi$.

Each set of data (1992, 1993, and 1994) used different calibration constants; therefore, each data set had its own efficiency that depended on its calibration constants.*

* The parameters can be found in the files REAL_SIM211, REAL_SIM212, REAL_SIM213, and REAL_SIM215 for 1992 (with the high threshold for the time-to-amplitude converter in drift chamber), 1992 (with lowered threshold), 1993, and 1994 respectively. These files are specified in the listing of parameters that is used to generate the desired events.

There was a set of calibration constants for each of two sets of data in 1992, a set for 1993, and another for 1994. Because double-tagging the event provided a clean and small sample, the Monte Carlo data was run with the same volume of clean $D^o\overline{D}^o$ events for all sets of data, using a relatively large number (e.g., for data set #215, 50,000 Monte Carlo events were generated and 20,107 were successfully double-tagged, Fig. 4.3-1) to minimize the statistical error.

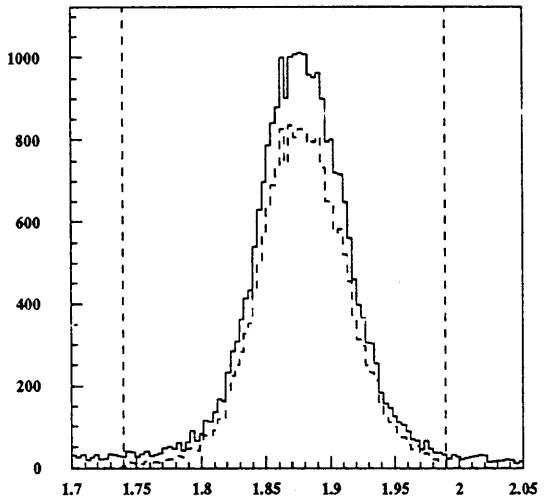

Figure 4.3-1 Invariant mass of the D^0 (in *GeV*). This shows Monte Carlo generated events (data set #215) that were successfully double-tagged, the dashed lines show events that made it through the final kinematic cuts (see 6.1). The average value is 1.878*GeV*. This analysis would yield an overall (i.e., without considering the angular distribution of the mesons) efficiency of 0.402.

5. Analysis

5.1. Physics of the *D* Meson

Some of the D meson parameters are listed in Table 1.1-1. The D^o meson decays only via weak processes, having a relatively small intrinsic width ($<<$ 1*eV*). This means that

the natural uncertainty in the mass spectrum is small and we therefore expect that the measured shape of the signal be dominated by the detector resolution.

The lowest order diagram for the D^o decay meson is shown below (Fig. 5.5-1). The weak hadronic decay of the charmed particle is based on the light-spectator-quark model. The mode we are studying is the Cabibbo-allowed decay process; essentially, the charm (c) quark decays into the lighter strange (s) quark through the emission of a virtual boson, the virtual boson then decays into the quark constituents of the π^+, as shown. [2]

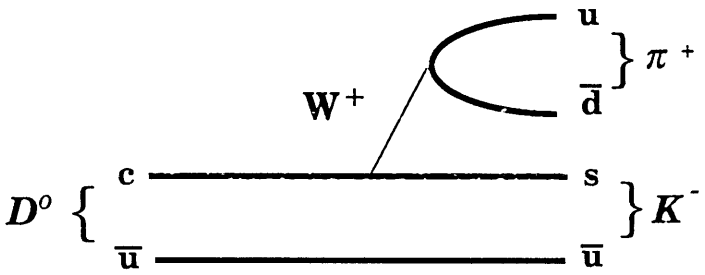

Figure 5.1-1 Cabibbo-allowed decay

Several types of D^o mesons can be pair produced at $4.03GeV$. These are shown in Table 5.1-1, along with relative information (N/A = Not Applicable).

TABLE 5.1-1 D^o Production Channels

Meson	Rest Mass (*MeV*)	Pair Production Threshold Energy (*GeV*)	D^o Channels	D^o Branching Fraction
D^o	1864.6 ± 0.5	3.729 ± 0.0005	N/A	N/A
D^{*o}	2006.7 ± 0.5	4.0134 ± 0.0005	$D^o\pi^o$ $D^o\gamma$	$(63.6 \pm 2.8)\%$ $(36.4 \pm 2.8)\%$
$D^{*\pm}$	2010.0 ± 0.5	4.020 ± 0.0005	$D^o\pi^+$	$(68.1 \pm 1.3)\%$
$D^{\pm}$	1869.4 ± 0.4	3.7388 ± 0.0004	N/A	N/A

Note that there are three channels for producing secondary D^o mesons via the decay of the more massive D^* mesons. Because we are seeking the production of D^o mesons directly from e^+e^- collisions, these channels constitute part of the background. In addition, note that there is also the doubly-Cabibbo-suppressed mode, $\overline{D}^o \rightarrow K^-\pi^+$, which we will consider negligible in our analysis. The aforementioned contributions to the background and how they are distinguished and/or removed from the signal will be discussed in a later section.

The momentum of the D^o mesons depend on the various processes of their production (e.g., whether these D^o mesons are decay products of the more massive D^* mesons or they are directly produced from e^+e^- collisions). The following table (5.1-2) lists the momentum ranges corresponding to these various processes. Monte Carlo simulations were used to determine the ranges in all except the direct production of D^o mesons and $e^+e^- \rightarrow D^{*+}\overline{D}^{*-} \rightarrow D^o\pi^+D^o\pi^-$. [8]

Table 5.1-2 Momentum Ranges for D^o Production from e^+e^- at 4.03 *GeV*

Production Mode	Momentum Range(*GeV*)
$e^+e^- \rightarrow D^o\overline{D}^o$	$p_D = 0.765$
$e^+e^- \rightarrow D^*\overline{D}^* \rightarrow D^o\pi^o\overline{D}^o\pi^o$	$0.004 \le p_D \le 0.308$
$e^+e^- \rightarrow D^*\overline{D}^* \rightarrow D^o\gamma\overline{D}^o\gamma$	$0.030 \le p_D \le 0.301$
$e^+e^-\ e^+e^- \rightarrow D^*\overline{D}^* \rightarrow D^o\pi^o\overline{D}^o\gamma$	$0.110 \le p_D \le 0.214$
$e^+e^- \rightarrow D^o\overline{D}^* \rightarrow D^o\overline{D}^o\pi^o$	$0.425 \le p_D \le 0.560$
$e^+e^- \rightarrow D^o\overline{D}^* \rightarrow D^o\overline{D}^o\gamma$	$0.375 \le p_D \le 0.663$
$e^+e^- \rightarrow D^{*+}\overline{D}^{*-} \rightarrow D^o\pi^+D^o\pi^-$	$p_{D,MAX} = 0.281$

The angular distribution for the production of D mesons has a straightforward dependence on the polar angle, θ, the angle between the e^+e^- beam and the D momentum vector, because it is a pseudoscalar. This means that the production amplitude is invariant with respect to coordinate system but it is still odd under reflection.

The production amplitude, $M_{D\overline{D}}$, is given by $M_{D\overline{D}} \propto \vec{\eta} \cdot \hat{p}$ where $\vec{\eta}$ is the polarization of the virtual photon and $\hat{p}$ is the unit 3-vector momentum of the D meson.

Then, to find the angular dependence of the cross section, we square the amplitude and sum over all polarization states of the virtual photon (for an unpolarized electron beam),

$$\frac{dN_{D\bar{D}}}{d\Omega} \propto \sum_{i,j} \eta_i \eta_j \hat{p}_i \hat{p}_j .$$

Using $\cos\theta = \hat{n} \cdot \hat{p}$, where $\hat{n}$ is the beam direction, together with the sum over the polarizations result, $\sum_{i,j} \eta_i \eta_j = \delta_{ij} - \hat{n}_i \hat{n}_j$, we find that

$$\frac{dN_{D\bar{D}}}{d\Omega} \propto (\delta_{ij} - n_i n_j)\hat{p}_i \hat{p}_j = 1 - (\hat{n} \cdot \hat{p})^2 = 1 - \sin^2\theta, \text{ or}$$

$$\frac{dN_{D\bar{D}}}{d\Omega} \propto \cos^2\theta.$$

5.2. Data Analysis

The data for all recorded events had the following things in common:

- at least three charged tracks reconstructed in the drift chamber OR at least two photon hits in the BSC,
- a total scalar momentum of greater than or equal to $1.5GeV$, and
- reconstructed tracks were within $20cm$ along z and within $2cm$ radially from the e^+e^- nominal interaction point.

Additional requirements are made in double-tagging the D^o mesons (see section 6.1).

5.2.1. Background

As mentioned in section 5.1.1, there are several channels at $4.03GeV$ from which D^o mesons are produced in addition to the direct production ($e^+e^- \rightarrow D^o\overline{D}^o$) we are attempting to measure. The additional modes would constitute the background for our analysis (see Table 5.1-1). The background can be broken up into two parts, that from secondary D^o mesons and that from the misidentification of decay products.

Much of the background processes were eliminated as we attempted to double-tag an event as $D^o\overline{D}^o$ using charge conservation and later in applying kinematic cuts. The muon shower counter eliminated events that had definitely identified muons. If data from

the shower counter had been available, it could have been used to detect direct gammas and gammas from neutral pion decays that came with the decay of D^* to D^o mesons.

Because the shower counter data was unavailable, removal of the background depended on the comparison of the Monte Carlo simulation of secondary D^o mesons and primary D^o mesons and also on the simulation of decay modes consisting of products that could be misidentified with those from the selected mode, $D^o \rightarrow K^-\pi^+$. The list of channels with secondary D^o mesons and their momentum ranges are in Table 5.1-2. The use of these momentum ranges along with final kinematic cuts to eliminate this type of background is discussed in section 6.1. Only the $D^o\overline{D}^* \rightarrow D^o\overline{D}^o\gamma$ listed presents a real problem where about 18% of these events fall within the final momentum cuts for the D^o mesons. However, we found that the background, including this mode, was essentially eliminated when we made tight enough mass cuts, momentum cuts, and back-to-back angle cuts. Figure 6.1-1 shows the possible candidates for the signal as a sum of the masses of the D mesons (mass(D^o)+mass($\overline{D}^o$) = $3.728GeV$).

A primary misidentification is that of kaons and pions because at $4.03GeV$, the momenta of these decay products are large when compared to their rest masses, giving a reconstructed invariant mass of the D^o meson that closely approximates the expected value regardless of which we call the pion or kaon. Our final identification of the kaons and pions was based on weighted information from the TOF system, the dE/dx measurements, and the muon shower counter. However, the sparseness of the final data set allowed us to choose the best $D^o\overline{D}^o$ pair as that having the smallest difference between the reconstructed energy of the system and the given center-of-mass energy as well as having its D momentum vectors closest to being back-to-back.

There are several other misidentifications possible in this analysis. For example, we might misidentify the set of decay products, $K^-\pi^+\pi^o$, as $K^-\pi^+$ with a missing π^o. In terms of just counting $D^o\overline{D}^o$ pairs, confusing kaons and pions would not be much of a problem except that the efficiencies for detecting the particles are different. However,

because in the end we use a total efficiency for the reconstructed D^o meson and choose the best pair that satisfies the kinematic cuts as well as the best back-to-back-ness, and best conservation of energy, the error involved in misidentifying the kaons and pions is negligible.

The following is a list for processes with potential for misidentification as our selected mode:

1. $D^o \rightarrow K^-K^+$ where one kaon was called a pion,
2. $D^o \rightarrow \pi^-\pi^+$ where one pion was called a kaon,
3. $D^o \rightarrow K^-\pi^+\pi^o$ and $D^+ \rightarrow K^-\pi^+\pi^+$ in which the π^o or π^+ wasn't observed,
4. $D^o \rightarrow K^-e^+\nu$ or $D^o \rightarrow K^-\mu^+\nu$ in which e^+ or μ^+ was called a pion.

The tightness of our kinematic cuts together with the Monte Carlo analysis of these decay processes let us safely ignore the processes listed above. Background from the doubly-Cabibbo-suppressed channel and the modes that decayed to two pions or two kaons were safely ignored because their branching fractions were all less than 0.01 times the selected mode (see Table 1.1-3).

6. The Measurement

6.1. Selection and Identification of $D^0\overline{D}^0$ Events

The selection of all charm events had to meet the criteria as specified in section 5.2.

To reconstruct the D^o mesons from kaons and pions, we specified the following general boundaries in the algorithm for the analysis of a typical event.

- To eliminate D^o meson candidates that were NOT a result of e^+e^- collision (such as cosmic rays or interactions between beam and gas) as well as tracks that were from D^o meson secondary decays (such as kaon decay, $K^o \rightarrow \pi^+\pi^-$), we required the track to be within $15cm$ along the z direction and radially, within $2cm$ of the nominal interaction point.
- The polar angle, θ, between the track and the beam direction, had to satisfy $|\cos\theta| < 0.85$. Monte Carlo studies showed that there was a rapid decrease in the efficiency for tracks that did not satisfy this criteria (see section 5.2.3) and this was seen to be true for

reconstructed real data as well (i.e., the uncertainties increased and the reliability of data decreased).

We made additional requirements in addition to these because we were looking for D^o pairs by double-tagging the event.

We required the event to have a total charge of zero with 4 charged tracks. We looked at all possible pairings of these four particles to determine which best fit the expected values for the $D^o(\overline{D}^o)$ momentum ($p_D = 0.764GeV$), the $D^o(\overline{D}^o)$ invariant mass ($m_D = 1.864GeV$) and the beam constrained mass, $M_C = \sqrt{E_b{}^2 - P^2(D^o(\overline{D}^o))}$ where the beam energy is $E_b = 2.015GeV$ and $P(D^o(\overline{D}^o))$ is the measured magnitude of momentum of the $D^o(\overline{D}^o)$ candidate. Calculation of the constrained mass allows us to take advantage of the small uncertainty in the beam energy.

The combination of the final kinematic cuts listed below were what greatly reduced the data set:

1. An invariant mass, $M(D^o(\overline{D}^o))$: $1.74GeV < M(D^o(\overline{D}^o)) < 1.99GeV$,
2. Momentum magnitude, $P(D^o(\overline{D}^o))$: $0.58GeV < P(D^o(\overline{D}^o)) < 0.95GeV$, and
3. Back-to-back-ness such that $Cos(\theta_{12}) < -0.99$, where θ_{12} is the angle between the momentum vectors of the D^o and the $\overline{D}^o$ mesons.

See Figs. 6.1-1, 6.1-2, and 6.1-3 for the raw data without the above cuts.

The best pair, as mentioned before, was the one that conserved energy best and with the best back-to-back-ness.

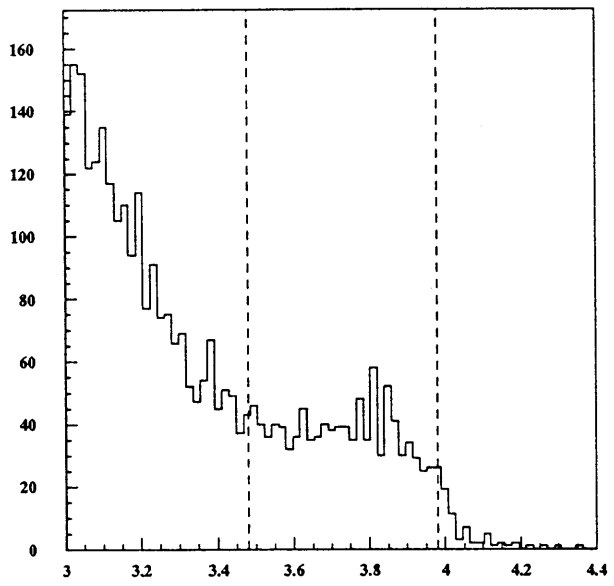

Figure 6.1-1 Sum of invariant masses of D^o and $\overline{D}^o$ candidates from all data sets. The dashed lines show final mass cuts, from 3.48*GeV* to 3.98*GeV*. The expected value is 3.728*GeV*.

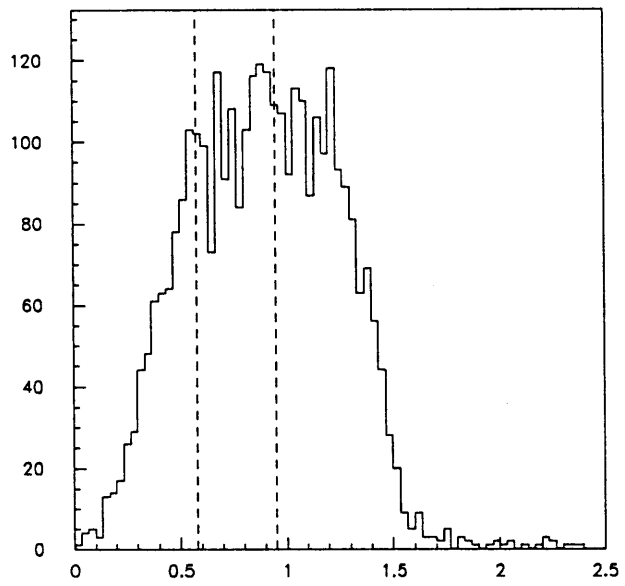

Figure 6.1-2 Magnitude of momentum of candidate D^o mesons from all data sets. The dashed lines show the final momentum cuts, from 0.58*GeV* to 0.95*GeV*. The expected value is 0.765*GeV*

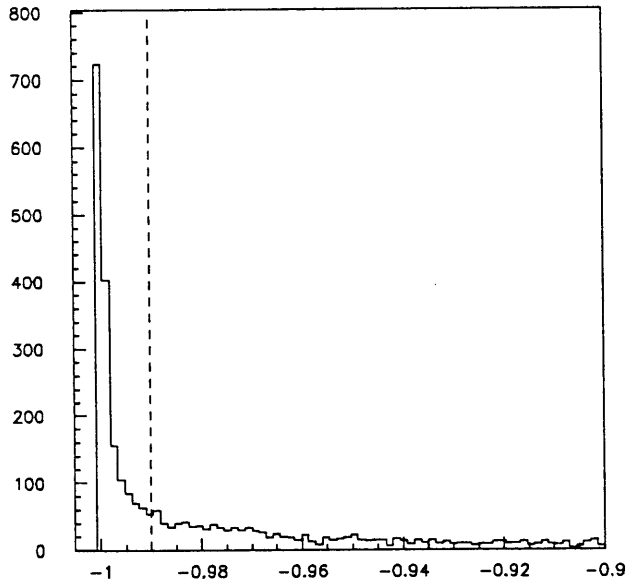

Figure 6.1-3 Cos(θ_{12}) of candidate $D^o\,\overline{D}^o$ pairs. The dashed line once again indicates the final cut in the back-to-back angle, at Cos(θ_{12})= -0.99. We expect the mesons to be back-to-back, therefore, the expected value is Cos(θ_{12})=-1.0.

6.2. The $N_{D\overline{D}}$ Measurement

The final data set consisted of 15 events. Each event was then corrected by its angular/kinematic efficiency, $\varepsilon(Cos\,\theta_D^i, \phi_D^i)$. The number of reconstructed $D^o\overline{D}^o$ pairs from the $D^o \to K^-\pi^+$ ($\overline{D}^o \to K^+\pi^-$) decay mode that were observed is then the sum of these corrected events, $N_{D\overline{D}}^{obs}$,

$$N_{D\overline{D}}^{obs} = \sum_{i=1}^{15}\left[1/\,\varepsilon(Cos\,\theta_D^i, \phi_D^i)\right] = 33.24$$

(final error will be discussed in the appendix).

To find the total number of $D^o\overline{D}^o$ pairs, $N_{D\overline{D}}$, each D^o ($\overline{D}^o$) has a branching fraction of $B(D^o \to K^-\pi^+) = B(\overline{D}^o \to K^+\pi^-) = 0.0401$, therefore,

$$N_{D\overline{D}} = N_{D\overline{D}}^{obs} / B^2(D^o \to K^-\pi^+) = 20{,}672.69.$$

This is the true number of primary $D^o\overline{D}^o$ pairs. Using this, we can now turn to the calculation of the exclusive $D^o\overline{D}^o$ pair production cross section.

6.2.1. The Exclusive $D^o\overline{D}^o$ Production Cross Section at $4.03GeV$

In this experiment, the electron and positron bunches were accelerated to $2.015GeV$, giving us a center-of-mass energy of $4.03GeV$. The volume of data is quoted in units of inverse barns, called the total integrated luminosity, L. The value for this analysis is $22.7pb^{-1}$. This quantity is related to the cross section, $\sigma_{D\overline{D}}$, and the number of primary $D^o\overline{D}^o$ pairs, $N_{D\overline{D}}$=20,672.69, by $N_{D\overline{D}} = \sigma_{D\overline{D}}L$ or

$$\sigma_{D\overline{D}} = N_{D\overline{D}} / L$$

We find our $D^o\overline{D}^o$ production cross section to be $\sigma_{D\overline{D}} = (0.91 \pm 0.31)nb$.

7. Conclusion

We find that the measurement of the exclusive $D^o\overline{D}^o$ pair production cross section at $4.03GeV$ can be simplified by using tight kinematic cuts, therefore dispensing with particle identification based on the TOF and dE/dx information; we did include the information from the muon counter to veto events with definitely identified muons. From a total integrated luminosity of $27pb^{-1}$, we were able to find 15 double-tagged events, giving us an exclusive production cross section of $\sigma_{D\overline{D}} = (0.91 \pm 0.31)nb$. Although it is about 3 standard deviations larger than the 1982 measurement by the MARK II collaboration, we did double-tag the events, greatly purifying the final data set (when compared to a single-tag analysis). In addition, we also had a much larger volume of data to work with than any of the other mentioned analyses.

8. APPENDIX: Error Analysis

To find the error in our cross section, we used the following formulas.

Given that the cross section is

$$\sigma_{D\bar{D}} = [\sum_{i=1}^{X}(N_i / \varepsilon_i)] / (B^2 L),$$

where N_i is the number of $D^o\bar{D}^o$ pairs that decayed via the $K\pi$ mode in the i-th efficiency bin, ε_i is the efficiency for the i-th bin, X is the total number of raw events, B is the branching fraction and L is the total integrated luminosity,

$$\delta\sigma_{D\bar{D}} = \sqrt{\left(\frac{\partial\sigma_{D\bar{D}}}{\partial B}\delta B\right)^2 + \left(\frac{\partial\sigma_{D\bar{D}}}{\partial L}\delta L\right)^2 + \sum_{j=1}^{X}\left(\frac{\partial\sigma_{D\bar{D}}}{\partial N_j}\delta N_j\right)^2 + \sum_{j=1}^{X}\left(\frac{\partial\sigma_{D\bar{D}}}{\partial \varepsilon_j}\delta\varepsilon_j\right)^2}.$$

Using

$$\frac{\partial\sigma_{D\bar{D}}}{\partial B}\delta B = -2\sigma_{D\bar{D}}\frac{\delta B}{B}$$

$$\frac{\partial\sigma_{D\bar{D}}}{\partial L}\delta L = -\sigma_{D\bar{D}}\frac{\delta L}{L}$$

$$\sum_{j=1}^{X}\left(\frac{\partial\sigma_{D\bar{D}}}{\partial N_j}\delta N_j\right)^2 = \sum_{j=1}^{X}\left(\frac{1}{\varepsilon_j}\frac{\delta N_j}{B^2 L}\right)^2 = \sum_{j=1}^{X}\left(\frac{\sqrt{N_j}}{B^2 L\varepsilon_j}\right)^2$$

$$\sum_{j=1}^{X}\left(\frac{\partial\sigma_{D\bar{D}}}{\partial\varepsilon_j}\right)^2 = \sum_{j=1}^{X}\left(\frac{-\delta\varepsilon_j}{B^2 L\varepsilon_j^2}\right)^2$$

we find that

$$\delta\sigma_{D\bar{D}} = \sqrt{\left(2\sigma_{D\bar{D}}\frac{\delta B}{B}\right)^2 + \left(\sigma_{D\bar{D}}\frac{\delta L}{L}\right)^2 + \sum_{j=1}^{X}\left(\frac{\sqrt{N_j}}{B^2 L\varepsilon_j}\right)^2 + \sum_{j=1}^{X}\left(\frac{\delta\varepsilon_j}{B^2 L\varepsilon_j^2}\right)^2}.$$

We use X=15, $\delta B = 0.0014$, $\delta\varepsilon_j \approx 0 \forall j$ because of the size of the Monte Carlo data set relative to the raw data (~20,000 observed Monte Carlo events compared to 15 observed

raw data events), $\delta N_j = 1 \forall j$ (using Poisson statistics for counting, where for each bin, j, we had only one raw event, so that $\delta N_j = \sqrt{N_j} = 1$ [9]) and the error in the luminosity, $\delta L = 0.03L = 681 nb^{-1}$.

Then

$$\delta\sigma_{D\bar{D}} = \sqrt{\left(2\sigma_{D\bar{D}}\frac{\delta B}{B}\right)^2 + \left(\sigma_{D\bar{D}}\frac{\delta L}{L}\right)^2 + \frac{1}{B^4 L^2}\sum_{j=1}^{x}\left(\frac{1}{\varepsilon_j}\right)^2} = \pm 0.31.$$

9. Acknowledgements

I would like to thank my parents, Vincent and Juanita Valdes, for always being there, no matter what.

I would like to extend my appreciation to Professor Richard Yamamoto. He gave me the opportunity to start this project; he saw me through the worst parts right to the end. I would like to thank him for taking the time to read my drafts, to offer advice, to take the time to explain things, and to always have suggestions of other things we could try to clarify what we saw or to solve existing problems. I would like to thank him for the courage to suggest things even when I did not want to try anything else. He took it as fact that I would finish and it worked!

I would also like to thank Oliver Bardon and Ray Cowan for their immense help; in paticular, for setting up the software, for helping with all subsequent problems I encountered in learning to use the software, and for sharing their experiences and know-how.

I would like to thank Jim Quigley , who was always willing to help with all the 'last-minute' things that always go wrong.

I would like to thank Professor Ulrich Becker for taking the time to officially read my thesis. I would like to thank Ms. Peggy Berkovitz, who always knew what else had to be done and how to do it. I would like to thank Professor George Koster, for being supportive and making sure I had the means to finish. I would like to thank Professor Nihat Berker, who always knew what to say to me, especially when things were not all that great.

References

1. *Particle Physics Booklet*, from the *Review of Particle Properties*, Physical Review, **D50**, 1173 (1994).

2. Schindler, R.H., et al, Phys Rev **D24**, Num 1, (1 July 1981) 78.

3. Coles, M.W., et al., Phys. Rev. **D26**, Num 9, (1 Nov 1982) 2190.

4. Baltrusaitis, R.M., et al, PRL **56** (19 May 1986) 2140.

5. Bai, J.Z., *et. al.*, 'The BES Detector', *Nuclear Instruments and Methods in Physics and Research*, **A 344**, (1994), 319.

6. Http://wwwpub.utdallas.edu/~joe/hepweb/besdocs/bestech.html.

7. Perkins, D. H., *Introduction to High Energy Physics*, 3d ed., Addison-Wesley Publishing Company, Inc. (Menlo Park), (1987).

8. Bardon, Oliver, MIT PhD thesis, *Measurement of the D^{*+} Branching Fractions*.

9. Taylor, John, R., *An Introduction to Error Analysis*, University Science Books, 1982.